Journal of Turbulence
Vol. 00, No. 00, 2009, 1–22

[a]Department of Aeronautics and Institute of Mathematical Sciences, Imperial College London, London, SW7 2AZ, U.K.; [b]*Aeronautics and Astronautics, School of Engineering Sciences, University of Southampton, Highfield, Southampton, SO17 1BJ, U.K.*

ISSN: 1468-5248 (online only)

DOI: 10.1080/14685240YYxxxxxxx
http://www.informaworld.com

Journal of Turbulence
Vol. 00, No. 00, 2009, 2–22

RESEARCH ARTICLE

Acceleration in turbulent channel flow

L. Chen[a], S. W. Coleman[a], J. C. Vassilicos[a†] and Z. Hu[b]

(*15 January 2010*)

We use Direct Numerical Simulations of turbulent channel flow to study the acceleration $\boldsymbol{A}$ corresponding to the full fluid velocity $\boldsymbol{u}$ and the acceleration $\boldsymbol{a}$ corresponding to the fluctuating velocity $\boldsymbol{u}' \equiv \boldsymbol{u} - \langle \boldsymbol{u} \rangle$ where $\langle \boldsymbol{u} \rangle$ is the mean flow. The mean acceleration $\langle \boldsymbol{A} \rangle = \langle \boldsymbol{a} \rangle$ is not zero, and the fluctuations of the convective and local parts of $\langle \boldsymbol{A} \rangle$ around their means approximately cancel in the intermediate log-like layer. The motions of stagnation points where $\boldsymbol{u}' = 0$ are controlled by $\boldsymbol{a}$. In this intermediate layer, the fluctuations of $\boldsymbol{a}$ around its mean come predominantly from the fluctuations of its local part. Stagnation points move with an average velocity which equals the average fluid velocity at these points. The fluctuations around this average stagnation point motion decrease in the log-like layer with increasing distance from the wall.

1. Introduction

It is well known (e.g. [1]) that, in turbulent channel flows for example, as the Reynolds number increases to infinity, the ratio of the channel width h to the wall unit distance δ_ν also increases to infinity. As a result, an intermediate range of distances z from the channel walls forms where $\delta_\nu \ll z \ll h/2$. Stripped to its bare essentials, the main assumption behind the intermediate asymptotics which lead to the form of the mean velocity profile in this intermediate range is this: as the Reynolds number tends to infinity, *something* is asymptotically independent of both h and the fluid's kinematic viscosity ν in this intermediate range. This *something* is usually taken to be the mean shear $\frac{d}{dz}U$ (where U is the mean flow velocity and z is the wall-normal coordinate). In this case, the immediate consequence of the intermediate asymptotic assumption is that, in the intermediate range $\delta_\nu \ll z \ll h/2$,

$$\frac{d}{dz}U \approx \frac{u_\tau}{\kappa z} \tag{1}$$

where u_τ is the skin friction velocity and κ is the von Karman constant. The famous log law of the wall follows directly by integration.

However, a recent work by [2] advances the idea that this *something* should in fact be the eddy turnover time $\tau \equiv E/\epsilon$ where E is the average kinetic energy per unit mass of the turbulent velocity fluctuations and ϵ is the dissipation rate of this average kinetic energy per unit mass. In this case, the immediate consequence of the intermediate asymptotic assumption is that, in the intermediate range $\delta_\nu \ll z \ll h/2$,

$$\tau \approx \frac{3}{2}\kappa_s \frac{z}{u_\tau} \tag{2}$$

*Corresponding author. Email: j.c.vassilicos@imperial.ac.uk

in terms of the constant of proportionality $\frac{3}{2}\kappa_s$ where κ_s is the stagnation point von Karman coefficient.

[2] combined this reformulated intermediate asymptotic assumption with (i) a local balance between energy production and dissipation [3] and with (ii) the fact that, in turbulent channel flows, the energy production takes the asymptotic form $u_\tau^2 \frac{d}{dz}U$ in the limit $h/\delta_\nu \to \infty$ and in the intermediate range $\delta_\nu \ll z \ll h/2$ as a result of the z-integrated momentum balance in the direction of the mean flow. They were therefore led to the conclusion that, in this intermediate range,

$$\frac{d}{dz}U \approx \frac{u_\tau}{\kappa_s z}(2E_+/3) \tag{3}$$

where $E_+ \equiv E/u_\tau^2$. If Townsend's inactive motions (see [4]) do not introduce a z and/or a Reynolds number dependence on E_+ in the present intermediate asymptotic limit, then their conclusion is the same as the usual one, i.e. equation (1). However, there are no reasons to expect Townsend's inactive motions not to have such an impact on E_+. Using the high Reynolds number turbulent channel flow data which [5] obtained by Direct Numerical Simulations (DNS), Dallas *et al* (2009) found better support for (3) than for (1), with $E_+ \sim z_+^{-2/15}$ in the intermediate range ($z_+ \equiv z/\delta_\nu$).

Dallas *et al* (2009) went on to argue that $\tau \approx \frac{3}{2}\kappa_s \frac{z}{u_\tau}$ implies a particular distribution in space of the instantaneous stagnation points of the turbulent fluctuating velocity $\boldsymbol{u}' \equiv \boldsymbol{u} - \langle \boldsymbol{u} \rangle$ where $\langle \boldsymbol{u} \rangle$ is the mean value of the fluid velocity $\boldsymbol{u}$ at a given distance from the channel walls. Specifically, they argued that $\tau \approx \frac{3}{2}\kappa_s \frac{z}{u_\tau}$ implies a number density n_s of such stagnation points which is inversely proportional to z_+ in the intermediate range $\delta_\nu \ll z \lesssim h/2$, i.e.

$$n_s \approx \frac{C_s}{\delta_\nu^3} z_+^{-1} \tag{4}$$

where $C_s \propto 1/\kappa_s$. They found good supporting DNS evidence for this inverse power-law relation in the range $\delta_\nu \ll z \lesssim h/2$.

Stagnation points are objectively and unambiguously well-defined quantities which are bound to be related to coherent structures. Numerous types of coherent structures have been proposed to explain experimentally observed phenomena in turbulent shear flow. However, the study of the nature and dynamical influence of coherent structures, as well as their own evolutionary dynamics, remains an open research question. Much of this difficulty comes in the myriad of structures which can be defined, though not without ambiguities (horseshoe- and hairpin-eddies, pancake- and surfboard-eddies, typical eddies, vortex rings, mushroom-eddies, arrowhead-eddies, etc.) [6]. In this context, the relation between the spatial distribution of velocity stagnation points and the mean flow profile is valuable. A motivation to study the motions of these stagnation points follows immediately from their unambiguous definition and relations to coherent structures and their importance in underpinning the mean flow profile. These stagnation points are of course not static and their motions therefore reflect coherent flow structure dynamics behind mean flow profiles. The definition of the velocity $\boldsymbol{V}_s$ of stagnation points (as opposed to the fluid velocity at stagnation points) was introduced by [7]:

$$\frac{\partial}{\partial t}\boldsymbol{u}' + \boldsymbol{V}_s \cdot \boldsymbol{\nabla}\boldsymbol{u}' = 0 \tag{5}$$

where $\boldsymbol{u}' = 0$. Hence, the fluid acceleration $\boldsymbol{a} \equiv \frac{\partial}{\partial t}\boldsymbol{u}' + \boldsymbol{u}' \cdot \boldsymbol{\nabla} \boldsymbol{u}'$ controls the motions of stagnation points and, specfically,

$$\boldsymbol{a} = -\boldsymbol{V}_s \cdot \boldsymbol{\nabla} \boldsymbol{u}' \tag{6}$$

at stagnation points. As a result, the motions of stagnation points offer in turn an immediate motivation for the study of acceleration statistics in a turbulent channel flow.

Of course, motivations to study acceleration statistics are wider and abound. The acceleration of a fluid element is perhaps the most direct and basic representation of fluid motion, reflecting the resultant of all forces acting on the fluid. As a result acceleration is of great interest for a variety of reasons, ranging from studies of fine scale intermittency [8] to applications in Lagrangian modelling of turbulence and turbulent dispersion [9, 10].

As the material derivative of the velocity vector $\boldsymbol{u}$, the acceleration appears on the left hand side of the incompressible Navier-Stokes equations

$$\boldsymbol{A} \equiv \frac{D\boldsymbol{u}}{Dt} = \frac{\partial \boldsymbol{u}}{\partial t} + \boldsymbol{u} \cdot \nabla \boldsymbol{u} = \frac{-1}{\rho} \nabla p + \nu \nabla^2 \boldsymbol{u}, \tag{7}$$

where p is the pressure and ρ is the fluid density. Previous acceleration studies have focused on homogeneous isotropic turbulence (HIT). The first studies of acceleration were performed using DNS of HIT [11] and were continued by [12], [8] and [13]. On the experimental side it has only been recently possible to perform direct Lagrangian measurements of acceleration by particle tracking [14–16]. Many of these studies have been concerned with the scaling of the acceleration. For instance, [14] observe Kolmogorov scaling at high Reynolds numbers. On the other hand [17] has developed a detailed and careful analysis which gives the scaling of acceleration variance at any Reynolds number and argues that Kolmogorov scaling cannot be observed at any Reynolds number. More recently [18] have reported hot wire mesurements of acceleration from field experiments at Taylor Reynolds numbers Re_λ up to 10^4 and do not find Kolmogorov scaling of the acceleration variance.

This scaling issue depends very sensitively on the so called random Taylor or sweeping decorrelation hypothesis, first proposed by [19], which states that in high Reynolds number turbulence the dissipative eddies flow past an Eulerian observer in a time which is much smaller than the characteristic timescale associated with their dynamics and which is determined by the sweeping of small eddies by large ones. [13] explains how this hypothesis means that the local and convective accelerations, $\boldsymbol{A}_l \equiv \frac{\partial \boldsymbol{u}}{\partial t}$ and $\boldsymbol{A}_c \equiv \boldsymbol{u} \cdot \nabla \boldsymbol{u}$ tend to anti-align as Reynolds number increases and thereby cancel much of each other so that $\boldsymbol{A} = \boldsymbol{A}_l + \boldsymbol{A}_c$ is much smaller and scales in a very different way than both $\boldsymbol{A}_l$ and $\boldsymbol{A}_c$. [13] found compelling DNS evidence that the sweeping decorrelation hypothesis is increasingly observed with increasing Reynolds numbers in HIT. [7] explained how the scaling of the stagnation point velocity $\boldsymbol{V}_s$ is in fact reflection of this sweeping decorrelation hypothesis.

The motivations to study acceleration statistics are all clearly closely interrelated: stagnation points of the fluctuating velocity field partly control the mean flow profile of turbulent channel flows. They result from small-scale turbulence dynamics which are, at least partly, reflected in the motions of these stagnation points. These are controlled by the acceleration and the velocity fluctuation gradient fields. The scalings of these two fields differ because of the sweeping of small dissipative eddies by large energy containing ones. This sweeping controls the scalings of the acceleration and of the stagnation point velocity $\boldsymbol{V}_s$. However, acceleration studies in

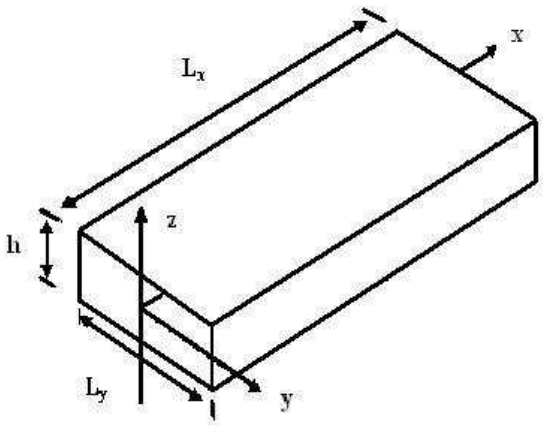

Figure 1. Sketch showing the geometry of the channel flow. Coordinates/velocities are x/u in the streamwise direction, y/v in the spanwise direction and z/w in the wall normal direction.

wall-bounded turbulence remain very scarce. For a start, $\boldsymbol{A}$ and $\boldsymbol{a}$ differ in such flows whereas they are they same in HIT, where $\langle \boldsymbol{u} \rangle = 0$.

To the authors' knowledge the only investigation of acceleration in wall-bounded turbulence is that of [20]. They used temporally resolved particle-image velocimetry measurements to determine the acceleration in a turbulent channel flow at friction Reynolds numbers $Re_\tau = 550$ and 1747. They found that the temporal derivative of the velocity in a frame moving with the bulk velocity $\boldsymbol{U}_b$ to be an order of magnitude smaller than the temporal derivative of the velocity in a frame not moving with respect to the wall. Although this gives an initial indication to the nature of sweeping in turbulent channel flow a more thorough investigation is needed.

This paper aims to give a description of the nature of acceleration in a turbulent channel flow. The layout of the paper is as follows. In §2 details of the DNS and of some of our numerical procedures are given before results are presented. In §3 we briefly confirm and discuss known mean velocity and vorticity profiles as well as equation (4) and its relation to the multiscale topography of the flow. Acceleration field decompositions and some of their basic properties are introduced in §4 so that §5 and §6 can follow with new results on various mean profiles of the various acceleration fields introduced in §4. In §7 we present statistics and profiles of the stagnation point velocities $\boldsymbol{V}_s$ and we conclude in §8.

2. Governing equations and summary of mumerical method

The governing equations of incompressible turbulent flow, the continuity and the momentum equation, are non-dimensionalized with the channel half height h and the friction velocity u_τ. A schematic of the notation for the channel geometry is given in Fig. 1: the mean flow is in the x-direction and the channel walls are normal to the z-axis.

The non-dimensional continuity and rotational form of the momentum equation can then be written as (using Einstein summation notation)

$$\frac{\partial u_j}{\partial x_j} = 0, \tag{8}$$

Table 1. Details of the two turbulent channel flow simulations. Re_τ is the friction Reynolds number, N_i the number of grid points in the i direction and L_x, L_y and h are shown in figure 1

Case	Re_τ	$N_x \times N_y \times N_z$	L_x	L_y	h
A	360	$256 \times 256 \times 161$	12	6	2
B	720	$512 \times 512 \times 321$	24	12	2

$$\frac{\partial u_i}{\partial t} = \epsilon_{ijk} u_j \omega_k + \delta_{1i}\Lambda - \frac{\partial \Pi}{\partial x_i} + \frac{1}{Re_\tau}\frac{\partial^2 u_i}{\partial x_j \partial x_j}. \tag{9}$$

Here ω_i is the ith vorticity component, $\omega_i = \epsilon_{ijk}\frac{\partial u_k}{\partial x_j}$, with ϵ_{ijk} being the permutation tensor; $Re_\tau = \frac{u_\tau h}{\nu}$ is the friction Reynolds number; $\Pi = p + u_i u_i/2$ is the modified non-dimensional pressure and $\delta_{1i}\Lambda$ is the driving mean pressure gradient.

Numerical solutions of the above equations are obtained as in [21] using the spectral method of [22], with Fourier methods used for spatial discretization in the streamwise and transverse directions and Chebyshev methods used in the wall normal direction. The pressure and viscous terms are treated implicitly to avoid extremely small time steps in the near-wall region. A third order Runge-Kutta scheme is used to integrate the convective terms. The '3/2 rule' is used for dealiasing whenever nonlinear quantities are required, with the additional wavenumbers generated by this process truncated.

This paper is concerned with two simulations in large computational domains at different Reynolds numbers ($Re_\tau = 360$ and 720). Details of the simulation are given in table 1. All statistics are collected only after the simulation has reached a statistically stationary state.

Reynolds decompositions of the velocity field, i.e. $\boldsymbol{u} = \langle \boldsymbol{u} \rangle + \boldsymbol{u'}$, where $\langle \boldsymbol{u} \rangle = (U(z), 0, 0)$, are obtained by calculating the mean flow numerically as $\langle \boldsymbol{u}(z_k) \rangle = \frac{1}{N_x N_z}\sum_{i=1}^{N_x}\sum_{j=1}^{N_y} \hat{\boldsymbol{u}}(x_i, y_j, z_k)$, $k = 1, \ldots, N_z$. The acceleration due to the fluctuating velocity was calculated both via $\boldsymbol{a} = \frac{\partial \boldsymbol{u'}}{\partial t} + \boldsymbol{u'}\cdot\nabla\boldsymbol{u'}$ and $\boldsymbol{a} = \boldsymbol{A} - \langle \boldsymbol{u} \rangle \cdot \nabla \boldsymbol{u} - \boldsymbol{u}\cdot\nabla\langle \boldsymbol{u} \rangle$ (see §4) using a simple first order finite difference for time derivatives. Both methods give indistinguishable statistics.

3. Mean velocity and vorticity profiles and the topography of turbulent channel flow

As a validation of our numerics, we check some standard statistics of the velocity field as first presented in the seminal paper [23]. The mean velocity is shown in figure 2, where the wall-normal coordinate is given in wall units $z_+ = z/\delta_\nu$ with $\delta_\nu = \nu/u_\tau$. The velocity is normalized by the friction velocity, $U_+ = U/u_\tau$, with $U = \langle u \rangle$ and $\langle \ldots \rangle$ denoting spatial averaging. Our data show the usual DNS agreement with $U_+ = z_+$ at very small values of z_+. Furthermore, $U_+ = \frac{1}{0.41}\log z_+ + 5.2$ provides an approximate fit of the data in a candidate intermediate z_+ region above 30 and well below Re_τ, as is also usual with such DNS data.

The root mean square (rms) values of velocity component fluctuations, u_{rms}, are shown in figure 3. [24] indicated that the Reynolds number effect on the turbulent intensity in the spanwise direction is significantly larger than in the other two directions. In the present study both spanwise and wall-normal rms velocity fluctuations increase with Reynolds number. However the rms value of the streamwise velocity fluctuations shows negligible change as we increase the Reynolds number, which is not consistent with [25]. We believe this difference results from the lower

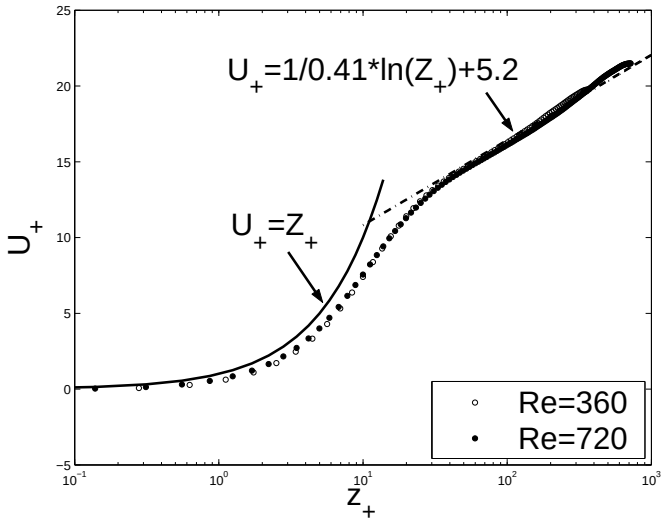

Figure 2. Mean velocity profile for both simulations.

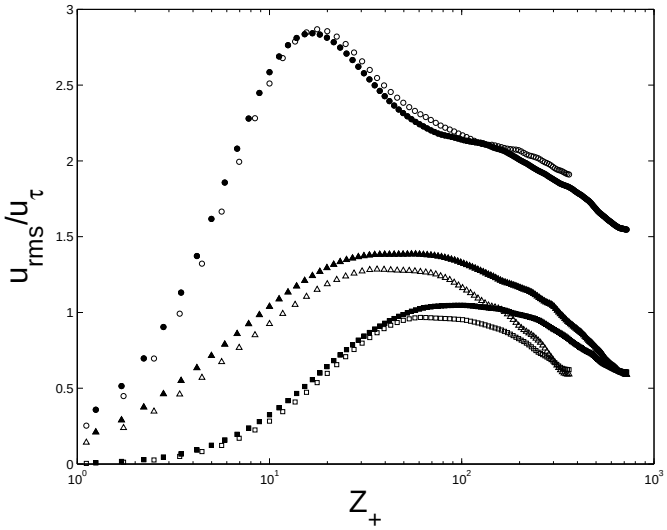

Figure 3. Root mean square value of turbulence intensity. Circles indicate streamwise, triangles spanwise and squares wall normal. Open and filled symbols are for $Re_\tau = 360$ and 720 respectively.

accuracy of the finite difference method compared to the spectral method employed here. It is also worth noting that the peak values of u_{rms} in the spanwise and wall normal directions move away from the wall in terms of wall units as Re_τ increases, whereas the peak value of the streamwise u_{rms} does not.

The rms of vorticity normalised by wall variables, i.e., $(\omega_+)_{rms} = \frac{\omega_{rms}\delta_\nu}{u_\tau}$ is shown in figure 4. The differences between the two Reynolds numbers are insignificant except in the near-wall region where the rms value of the vorticity increases with increasing Reynolds number. Note, in passing, how the flow is clearly not two-dimensional near the walls. At values of z_+ larger than about 30, all three vorticity curves more or less collapse on each other thus providing evidence of small-scale isotropy far enough away from the walls. Our results are in qualtitative agreement with those of [25] who studied turbulent channel flows at $Re_\tau = 160, 395$ and 640.

Finally, concerning the multiscale topography of channel flow turbulence, we confirm the finding (4) of [2] which was achieved with a very different DNS code. We follow [2] in locating stagnation points $\boldsymbol{u}' = 0$ numerically with a Newton-Raphson method underpinned by a fourth-order Lagrange interpolation. We then count the

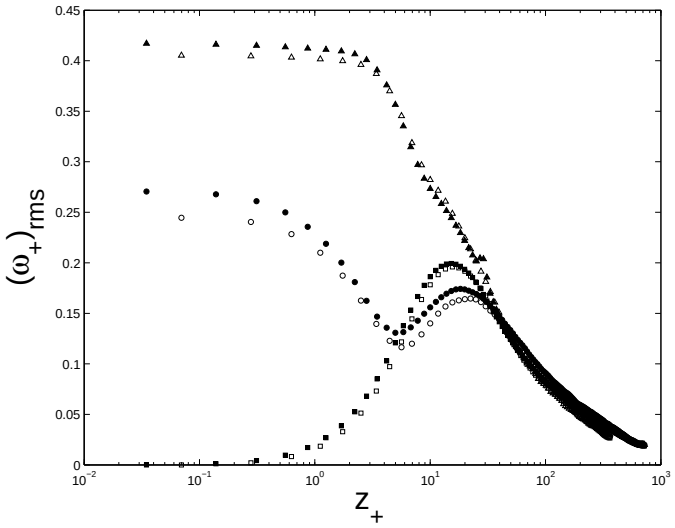

Figure 4. Root mean square value of vorticity normalised by wall variables. Circles indicate vorticity in the streamwise, triangles in the spanwise and squares in the wall normal directions. Open and filled symbols are for $Re_\tau = 360$ and 720 respectively.

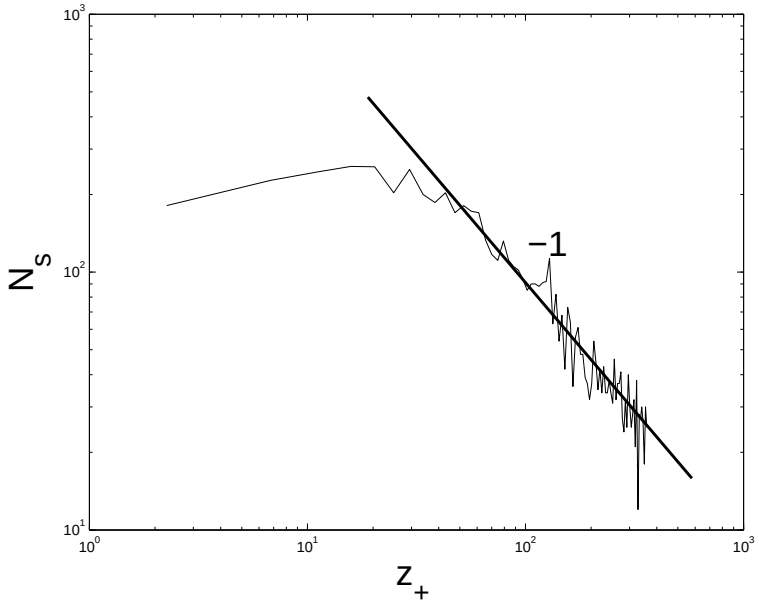

Figure 5. Number of zero-velocity points as a function of distance from the wall for $Re_\tau = 360$.

number N_s of stagnation points within a thin slab of dimension $L_x \times L_y \times \delta_z$, where δ_z is the thickness of the slab. Figure 5 shows how the number of velocity stagnation points increases from the wall and then decreases towards the centre of the channel, taking a peak at $z_+ = 20$. It is clear from figure 5 that the number density, $n_s = \frac{N_s}{L_x L_y \delta_z}$ of zero-velocity points in a thin slab of dimension $L_x \times L_y \times \delta_z$ (in this figure $\delta_z = \delta_\nu$) parallel to the wall and at a distance z from it, is in agreement with (4).

The decrease of the number of stagnation points with distance from the wall in the region $z_+ \geq 30$ is in qualitative agreement with the increase of streak size with distance from the wall in that same region (see figure 6) and with the schematic picture of multi-size attached eddies proposed in [26] (see figure 7). However, it cannot be expected that all stagnation points correspond to attached eddies as many of them must also result from small wall-free turbulent eddies. [27] showed

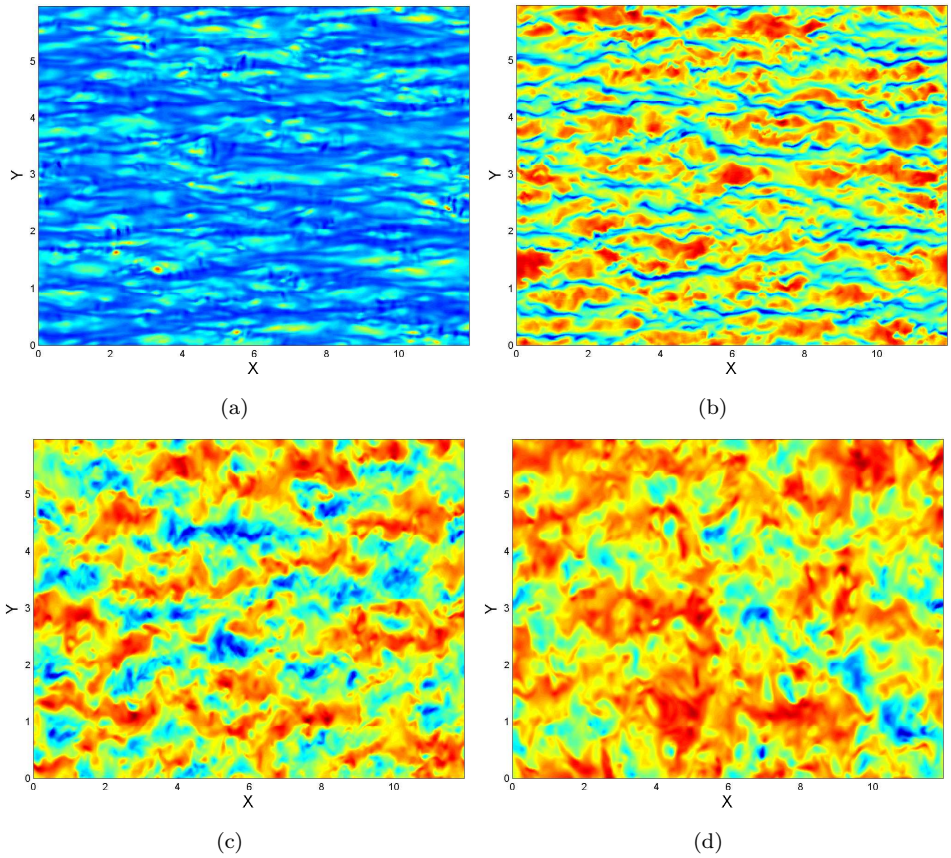

Figure 6. Contours of u at different distances from the wall for $Re_\tau = 360$. Blue denotes negative values and red denotes positive values. (a) $z_+ = 1$, (b) $z_+ = 27$, (c) $z_+ = 160$, (d) $z_+ = 360$.

that the number density of stagnation points in HIT is proportional to $(L/\eta)^2$ where L is the integral length-scale, $\eta \sim (\nu^3/\epsilon)^{1/4}$ and ϵ is the kinetic energy dissipation rate per unit mass. Assuming local HIT at a distance z from the wall in the region $z_+ \geq 30$, the number N_s of stagnation points within a thin slab of dimension $L_x \times L_y \times \delta_\nu$ can then be estimated as $N_s \approx \frac{L_x L_y \delta_\nu}{L_x^3} C_a(z_+)(L/\eta)^2$ where $L \sim z$, $\eta \sim (\nu^3/\epsilon)^{1/4} \sim \delta_\nu^{3/4} z^{1/4}$ (see [1]) and $C_a(z_+)/L_x^3$ is the number density of attached addies at a distance z from the wall. Comparing with $N_s \sim \frac{L_x L_y}{\delta_\nu^2} z_+^{-1}$ which results from (4), it then follows that $C_a/L_x^3 \sim \delta_\nu^{-3} z_+^{-5/2}$. This would be the scaling for stagnation points related to attached eddies. It is not the same as the scaling (4) for all stagnation points.

4. Acceleration field of turbulent channel flow

In the introduction we alluded to the fact that $\boldsymbol{A} \equiv \frac{\partial \boldsymbol{u}}{\partial t} + \boldsymbol{u} \cdot \nabla \boldsymbol{u}$ and $\boldsymbol{a} \equiv \frac{\partial \boldsymbol{u'}}{\partial t} + \boldsymbol{u'} \cdot \nabla \boldsymbol{u'}$ are different in turbulent channel flows even though they are equal in HIT where $\langle \boldsymbol{u} \rangle = 0$. In a statistically stationary turbulent channel flow where $\langle \boldsymbol{u} \rangle = (U(z), 0, 0)$ and $\frac{\partial \boldsymbol{u}}{\partial t} + \boldsymbol{u} \cdot \nabla \boldsymbol{u} = \boldsymbol{0}$,

$$\boldsymbol{A} = \boldsymbol{a} + \langle \boldsymbol{u} \rangle \cdot \nabla \boldsymbol{u} + \boldsymbol{u} \cdot \nabla \langle \boldsymbol{u} \rangle. \tag{10}$$

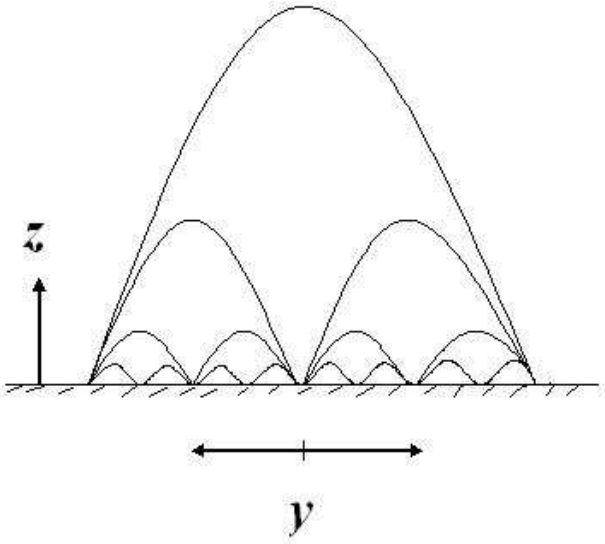

Figure 7. A conceptual sketch of attached eddies of varying distance from the wall.

This decomposition of the acceleration field has the property that

$$\langle \boldsymbol{A} \rangle = \langle \boldsymbol{a} \rangle \tag{11}$$

$$= -\frac{1}{\rho}\nabla\langle p \rangle + \nu\nabla^2\langle \boldsymbol{u} \rangle. \tag{12}$$

Furthermore, incompressibility and statistical stationarity imply that the first moments of the acceleration components give the Reynolds stress gradients, i.e.

$$\langle a_i \rangle = \frac{\partial}{\partial x_j}\langle u_j' u_i' \rangle. \tag{13}$$

Following [28] we also decompose each acceleration field $\boldsymbol{A}$ and $\boldsymbol{a}$ into local and convective accelerations, i.e. $\boldsymbol{A} = \boldsymbol{A}_l + \boldsymbol{A}_c$, where $\boldsymbol{A}_l = \frac{\partial \boldsymbol{u}}{\partial t}$ and $\boldsymbol{A}_c = \boldsymbol{u}\cdot\nabla\boldsymbol{u}$ and $\boldsymbol{a} = \boldsymbol{a}_l + \boldsymbol{a}_c$, where $\boldsymbol{a}_l = \frac{\partial \boldsymbol{u'}}{\partial t}$ and $\boldsymbol{a}_c = \boldsymbol{u'}\cdot\nabla\boldsymbol{u'}$. Note that of all these acceleration terms, only the total acceleration $\boldsymbol{A}$ and the convective "fully fluctuating" acceleration $\boldsymbol{a}_c$ are Galilean invariant. The Eulerian constituents $\boldsymbol{A}_l$ and $\boldsymbol{A}_c$ of the Lagrangian total $\boldsymbol{A}$ are not Galilean invariant, and neither are $\boldsymbol{a}$ and $\boldsymbol{a}_l$

Note also that $\langle \boldsymbol{A}_l \rangle = \langle \boldsymbol{a}_l \rangle = 0$ and that

$$\langle \boldsymbol{A} \rangle = \langle \boldsymbol{A}_c \rangle = \langle \boldsymbol{a} \rangle = \langle \boldsymbol{a}_c \rangle. \tag{14}$$

5. Mean acceleration profiles in turbulent channel flow

In this section we calculate the three average acceleration profiles $\langle A_x \rangle = \langle a_x \rangle$, $\langle A_y \rangle = \langle a_y \rangle$ and $\langle A_z \rangle = \langle a_z \rangle$ (as functions of z).

As explained in [1], assuming the turbulence to be statistically stationary and effectively homogeneous in all directions except z, the wall-normal mean momentum equation implies

$$\frac{\partial\langle p \rangle}{\partial x} = \frac{dp_w}{dx}, \tag{15}$$

where $p_w = \langle p(x,0,0)\rangle$ is the mean pressure on the bottom wall. From the streamwise mean momentum equation one obtains

$$\frac{d\tau}{dz} = \frac{dp_w}{dx}, \tag{16}$$

where the total shear stress $\tau(z)$ is given by

$$\tau = \rho\nu\frac{dU}{dz} - \rho\langle uw\rangle. \tag{17}$$

In the near-wall region, for fixed time and space, the normalised fluctuating velocity components $u_+ \equiv u/u_\tau$, $v_+ \equiv v/u_\tau$ and $w_+ \equiv w/u_\tau$ can be written as Taylor series expansions [1],

$$u_+ = b_1 z_+ + c_1 z_+^2 + \ldots, \tag{18}$$

$$v_+ = b_2 z_+ + c_2 z_+^2 + \ldots, \tag{19}$$

$$w_+ = c_3 z_+^2 + \ldots, \tag{20}$$

where the boundary conditions $u = v = w = 0$ and $\omega_z = 0$ at the wall have all been taken into account. The mean streamwise acceleration $\langle a_x\rangle = \frac{\partial}{\partial z}\langle uw\rangle$ and in the viscous sublayer $z_+ < 5$ it then follows that

$$\langle a_x\rangle = \frac{\partial}{\partial z}\langle uw\rangle \tag{21}$$

$$= -3\sigma\frac{u_\tau^2}{\delta_\nu}z_+^2, \tag{22}$$

where the non-dimensional coefficient $\sigma = b_1 c_3$ may be assumed to be independent of Reynolds number.

In the intermediate layer, $30 < z_+, z/h < 0.3$, if we assume a log law (1) for simplicity, i.e. $\frac{\partial^2 U_+}{\partial z_+^2} = -\frac{1}{\kappa}z_+^{-2}$, and do not take into account the correction (4) introduced by [2], then

$$\langle a_x\rangle = \frac{\partial}{\partial z}\langle uw\rangle \tag{23}$$

$$= \frac{2u_\tau^2}{h} - \nu\frac{u_\tau}{\delta_\nu^2\kappa}z_+^{-2} \tag{24}$$

$$= \frac{u_\tau^2}{\delta_\nu}\left(2\frac{\delta_\nu}{h} - \frac{1}{\kappa}z_+^{-2}\right). \tag{25}$$

where use has been made of the fact that $-\frac{1}{\rho}\frac{\partial<p>}{\partial x} = \frac{2u_\tau^2}{h}$. This implies, in particular, that as z_+ increases towards the centre of the channel, $\langle a_x\rangle \to \frac{2u_\tau^2}{h} \neq 0$. These estimates are in sufficiently good agreement with our simulations as shown in figures 5 and 9(a).

In the spanwise direction, we have

$$v\left(\frac{\partial u}{\partial x} + \frac{\partial v}{\partial y} + \frac{\partial w}{\partial z}\right) = 0 \tag{26}$$

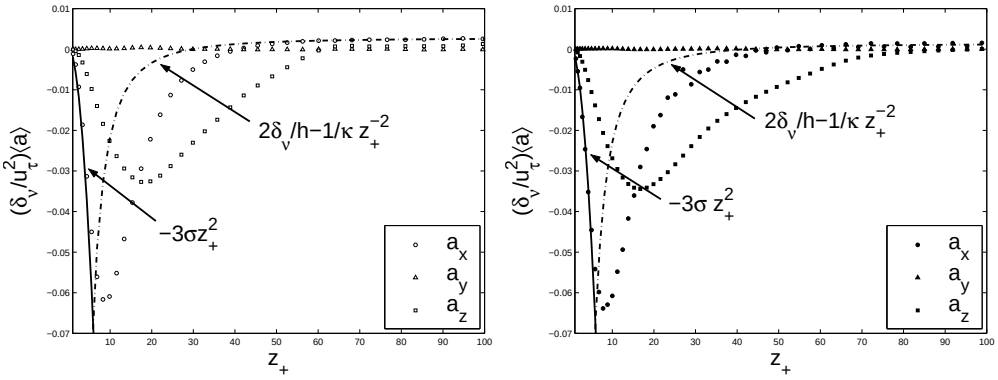

(a) $Re_\tau = 360$. (b) $Re_\tau = 720$.

Figure 8. Average acceleration profiles for all three acceleration components as indicated by the legend

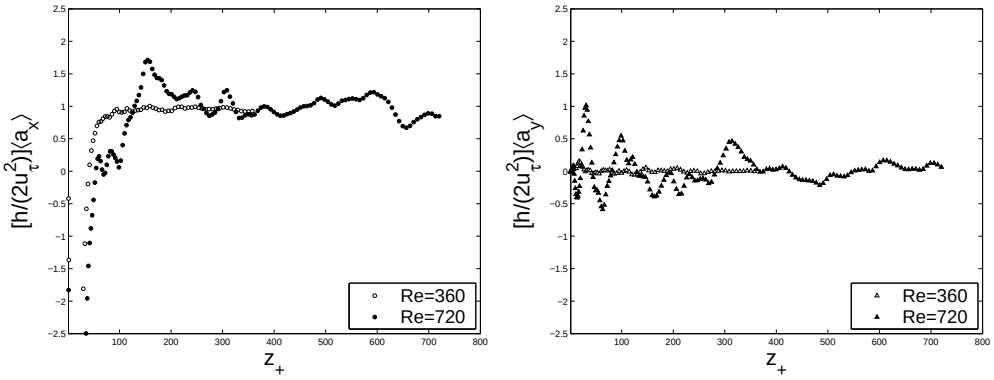

(a) (b)

Figure 9. Mean acceleration normalized by $2u_\tau^2/h$ in all three directions for $Re_\tau = 360$ and 720. (a) shows the streamwise direction and (b) the spanwise.

from the incompressibility condition. Substituting equation 26 into the definition $A_y = \frac{\partial v}{\partial t} + u\frac{\partial v}{\partial x} + v\frac{\partial v}{\partial y} + w\frac{\partial v}{\partial z}$, and averaging with the assumptions of statistical stationarity and homogeneity in the streamwise and spanwise directions, leads to

$$\langle A_y\rangle = \langle a_y\rangle = 0. \tag{27}$$

Similar analysis in the wall-normal direction under the same assumptions gives

$$\langle A_z\rangle = \langle a_z\rangle = \frac{\partial\langle w^2\rangle}{\partial z}. \tag{28}$$

This conclusion is also confirmed by our data as shown in figures 5 and 9(b). The Reynolds number dependencies appear insignificant in this data. The minimum value of the averaged streamwise acceleration appears at $z_+ = 9$ for both Reynolds numbers, whilst the minimum value of the averaged acceleration in the wall-normal direction is at $z_+ = 18$.

6. Quadratic mean acceleration profiles in turbulent channel flow

The Reynolds number scaling of the acceleration variance mentioned in the Introduction was first studied by [29] and [30] in the HIT case. By direct application of Kolmogorov scaling they obtained $\langle a_i a_j\rangle = a_0\epsilon^{3/2}\nu^{-1/2}\delta_{ij}$, where a_0 is a universal

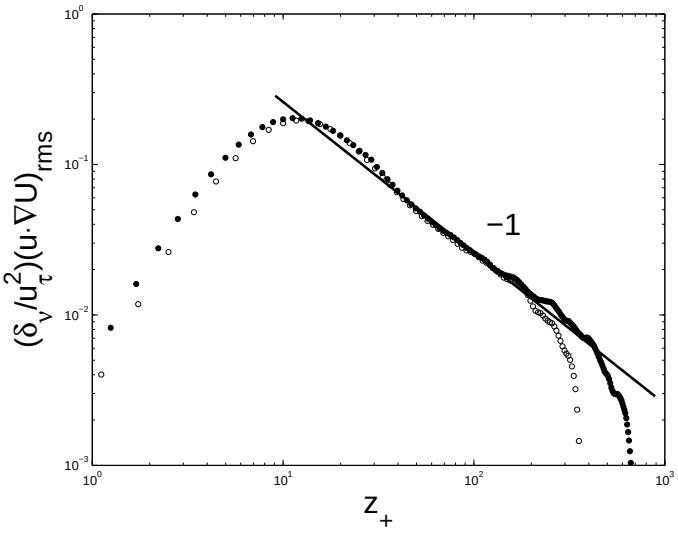

Figure 10. Rms value of $\boldsymbol{u'} \cdot \nabla U$. Open symbols indicate $Re_\tau = 360$ and filled symbols $Re_\tau = 720$.

constant independent of Reynolds number and ϵ is the kinetic energy dissipation per unit mass. It is only relatively recently that it has become possible to measure acceleration statistics in the laboratory, and the evidence resulting from these measurements as well as DNS and theoretical results are not in clear agreement with each other and are shedding doubt on the universality of a_0, including its presumed Reynolds number independence (see references mentioned in the Introduction).

In wall-bounded turbulence, the Reynolds number and the dissipation rate are effectively functions of distance to the wall so that arguments such as those of [29] and [30] lead to z-dependencies of acceleration variances. Also, there is more acceleration terms which are of interest in wall-bounded turbulence than in HIT. In turbulent channel flows we need to consider the variances of $\boldsymbol{A}$ and $\boldsymbol{a}$ and of the terms by which they differ, i.e. $\langle \boldsymbol{u} \rangle \cdot \nabla \boldsymbol{u'}$ and $\boldsymbol{u'} \cdot \nabla \langle \boldsymbol{u} \rangle$.

6.1. *Quadratic mean profiles of* $\langle \boldsymbol{u} \rangle \cdot \boldsymbol{\nabla u'}$ *and* $\boldsymbol{u' \cdot \nabla \langle u \rangle}$

We start with z-profiles of the variances of $\langle \boldsymbol{u} \rangle \cdot \nabla \boldsymbol{u'}$ and $\boldsymbol{u'} \cdot \nabla \langle \boldsymbol{u} \rangle$ in the intermediate layer where we may assume classical log-layer and Kolmogorov scalings to be good starting approximations. We therefore scale $\langle \boldsymbol{u} \rangle = (U, 0, 0)$ with u_τ, gradients of U with u_τ/z and gradients of turbulent velocity fluctuations $\boldsymbol{u'}$ with u_η/η where η is the Kolmogorov lengthscale at distance z from the wall and u_η is the Kolmolgorov velocity at that distance. Note however, that turbulent velocity fluctuations themselves are assumed to scale with u_τ.

Firstly we consider the term $\boldsymbol{u'} \cdot \nabla U$. Figure 10 shows that the rms of this term exhibits a clear power law dependence on z_+ with exponent -1 for $z_+ > 30$ and $z/h < 0.3$, i.e. the range where our DNS shows approximate agreement with the log law in figure 2. This is a range which increases with Reynolds number and this -1 power law can be seen as resulting directly from classical log-layer scalings, i.e. $\boldsymbol{u'} \cdot \nabla U \sim u_\tau u_\tau / z$.

Secondly, we consider the term $\langle \boldsymbol{u} \rangle \cdot \nabla \boldsymbol{u'} = U \frac{\partial}{\partial x} \boldsymbol{u'}$. On the basis of classical log-law and Kolmogorov scalings, the rms of this term can be estimated as follows

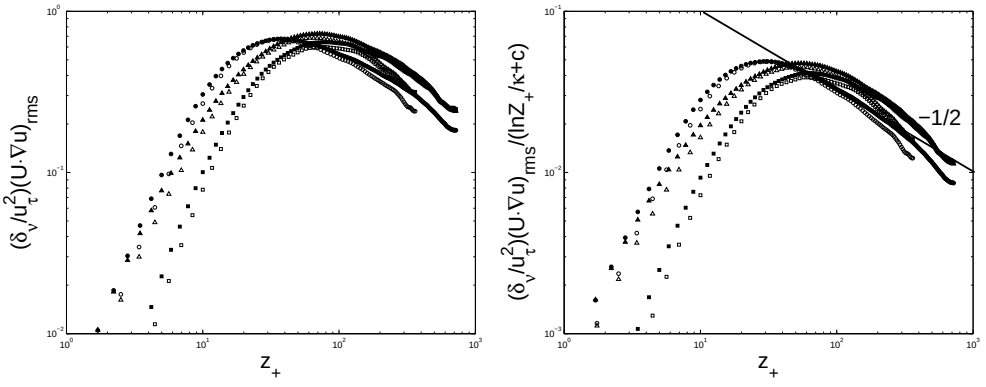

(a) (b)

Figure 11. Rms value of $\langle \boldsymbol{u} \rangle \cdot \nabla \boldsymbol{u'}$ (a) normalized by u_τ^2/δ_ν and (b) normalized by $\frac{u_\tau^2}{\delta_\nu}\left(\frac{\log z_+}{\kappa}+c\right)$. Circles indicate u, triangles v and squares w. Open symbols indicate $Re_\tau = 360$ and filled symbols $Re_\tau = 720$.

in the intermediate log-layer-like region:

$$\langle \boldsymbol{u} \rangle \cdot \nabla \boldsymbol{u'} \sim U \frac{u_\eta}{\eta} \tag{29}$$

$$\sim u_\tau \left(\frac{\log z_+}{0.41} + 5.2 \right) \frac{(\epsilon\eta)^{1/3}}{\eta} \tag{30}$$

$$\sim \left(\frac{\log z_+}{0.41} + 5.2 \right) \frac{u_\tau^2}{\delta_\nu} z_+^{-1/2}, \tag{31}$$

where we have made use of $\epsilon \sim u_\tau^3/z$, which is the classical expectation in the log-layer [1], and of $\eta \sim (\nu^3/\epsilon)^{1/4}$ and $\delta_\nu = \nu/u_\tau$. Figure 11 shows the z_+-profile of the rms of $\langle \boldsymbol{u} \rangle \cdot \nabla \boldsymbol{u'}$ for all three components of $\boldsymbol{u'}$ and for both Reynolds numbers. These rms profiles do not show clear agreement with our estimate (31) except, perhaps, for the streamwise component when plotted as $(\boldsymbol{U} \cdot \nabla u)/(\log z_+/\kappa + c)$ versus z_+ (see Figure 11b). However, it is clear that all the variances of each component of $\langle \boldsymbol{u} \rangle \cdot \nabla \boldsymbol{u'} = U \frac{\partial}{\partial x} \boldsymbol{u'}$ increase when moving away from the wall, then reach a peak and then decrease when moving towards the centre of the channel as qualitatively predicted by (31). The peak value in the streamwise direction is at $z_+ = 30$ and the peak values in the spanwise and wall-normal directions are at $z_+ = 70$.

6.2. *Quadratic mean profiles of A*

The total acceleration $\boldsymbol{A}$ can be decomposed as a sum of the local acceleration $\boldsymbol{A}_l = \partial \boldsymbol{u}/\partial t$, which expresses the rate of change of velocity $\boldsymbol{u}$ due to unsteadiness at a fixed point in space, and the convective acceleration $\boldsymbol{A}_c = \boldsymbol{u} \cdot \nabla \boldsymbol{u}$, which expresses the rate of change of velocity $\boldsymbol{u}$ due to convection past a fixed point in space.

Figure 12 shows the rms values of these total, local and convective accelerations. The rms values normalised by u_τ^2/δ_ν increase slightly with increasing Reynolds number. In the case of the higher Reynolds number $Re_\tau = 720$, the total acceleration $\boldsymbol{A}$ seems to be showing a power law scaling with distance from the wall in the intermediate log-like layer. The exponent of this power law is $-3/4$. This scaling can in fact be obtained from a Kolmogorov estimate of the rms of $\boldsymbol{A}$ as follows:

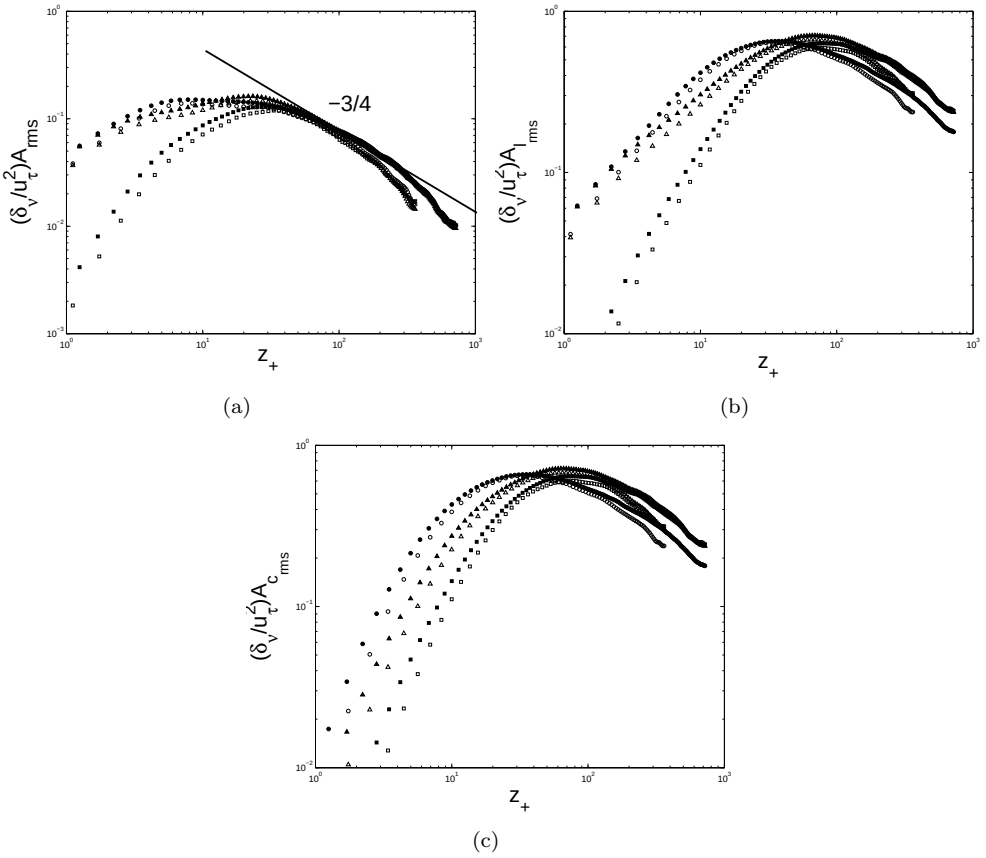

Figure 12. Rms value of acceleration terms. Circles indicate streamwise, triangles spanwise and squares wall normal. Open and filled symbols are for $Re_\tau = 360$ and 720 respectively. (a) total acceleration A_{rms}, (b) local acceleration $A_{l,rms}$ and (c) convective acceleration $A_{c,rms}$.

$$\boldsymbol{A} = \frac{D\boldsymbol{u}}{Dt} \tag{32}$$

$$\sim \frac{u_\eta^2}{\eta} \tag{33}$$

$$\sim \frac{(u_\tau z_+^{-1/4})^2}{\delta_\nu^{3/4} z_+^{1/4}} \tag{34}$$

$$\sim \frac{u_\tau^2}{\delta_\nu} z_+^{-3/4}. \tag{35}$$

This scaling seems to be confirmed by our simulations only in the higher Reynolds number case (figure 12a) presumably because of the larger span of the log-like layer. However, the z-profiles of the rms values of the local and convective accelerations have a less clear form. Note that, whilst the Galilean-invariant Lagrangian acceleration $\boldsymbol{A}$ may indeed be estimated by Kolmogorov scaling as above, the non-Galilean-invariant Eulerian accelerations cannot be estimated in this way. Instead, in the frame where the walls of the channel are not moving, one may write (in

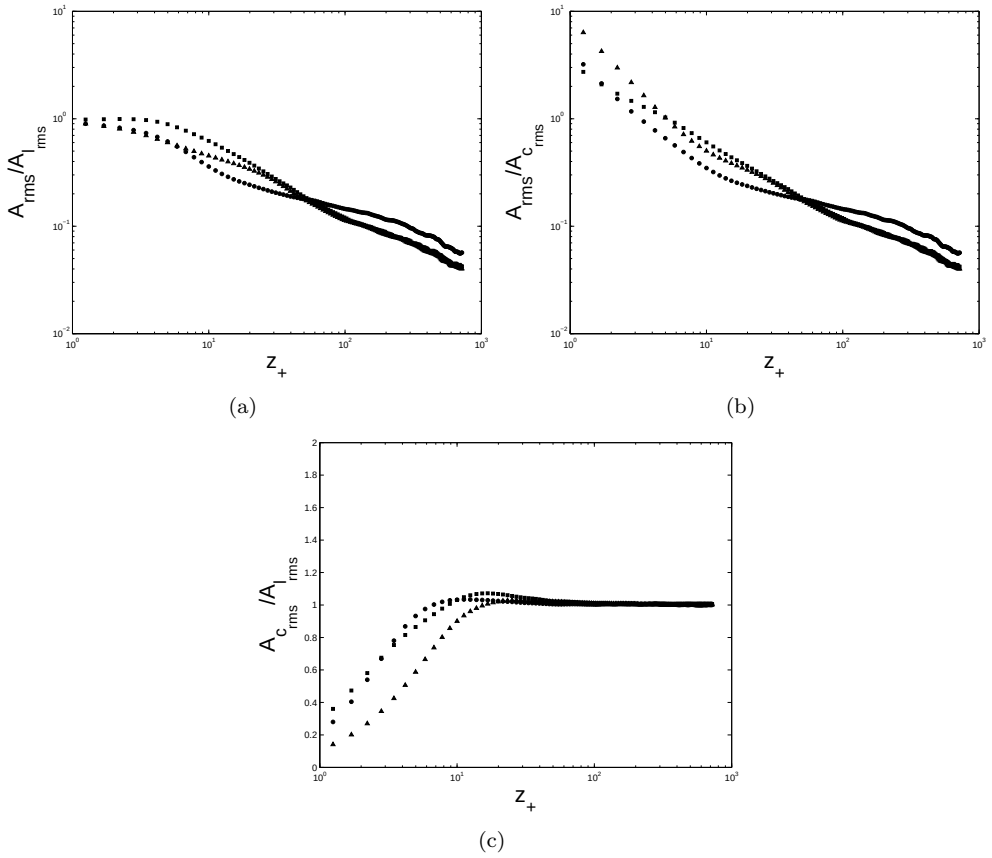

Figure 13. Ratio of rms values of acceleration terms. Circles indicate streamwise, triangles spanwise and squares wall normal. (a) $A_{rms}/A_{l,rms}$, (b) $A_{rms}/A_{c,rms}$ and (c) $A_{c,rms}/A_{l,rms}$. $Re_\tau = 720$.

terms of dimensionless constants α, β and β')

$$\boldsymbol{A}_c = \boldsymbol{u} \cdot \nabla \boldsymbol{u} \tag{36}$$

$$\sim u_\tau(\alpha \frac{u_\tau}{z} + \beta \frac{u_\eta}{\eta}) \tag{37}$$

$$\sim \frac{u_\tau^2}{\delta_\nu}(\alpha z_+^{-1} + \beta' z_+^{-1/2}). \tag{38}$$

with a neglected additive correction which has the same form but multiplied by $\log z_+$. A similar estimate can be made for the rms of $\boldsymbol{A}_l$. The dominant scaling term will be $z_+^{-1/2}$ at high enough Reynolds number and z_+, but our present Reynolds numbers are not high enough for this to be visible (see figure 12b and c where the rms values of $\boldsymbol{A}_l$ and $\boldsymbol{A}_c$ are plotted). However, one can venture to conclude from the above estimates that the rms of $\boldsymbol{A}_l$ and of $\boldsymbol{A}_c$ are larger than the rms of $\boldsymbol{A}$. This conclusion is confirmed by our simulations as shown in figure 13a and b.

[13] showed that in homogeneous isotropic turbulence the local and convective accelerations are approximately of the same magnitude but anti-aligned and thus cancel each other to produce a smaller total acceleration. This is predicted by the random Taylor or sweeping decorrelation hypothesis [19] whereby small eddies in turbulent flow are passively swept by large edddies. Figure 13 shows that something similar is the case in our simulations for the total acceleration $\boldsymbol{A}$ throughout the flow, except near the wall, i.e. $z_+ < 10$, where the fluctuations of the local acceleration $\boldsymbol{A}_l$ are the dominant contributor to the fluctuations of the total acceleration $\boldsymbol{A}$. It is clear from figures 13a and b, that the variance of the total acceleration $\boldsymbol{A}$

is much smaller than the variances of both $\boldsymbol{A}_l$ and $\boldsymbol{A}_c$ for $z_+ > 10$, whilst figure 13c shows that the variances of $\boldsymbol{A}_l$ and $\boldsymbol{A}_c$ have approximately the same magnitude for $z_+ > 10$. However, from sections 4 and 5 we know that $\langle \boldsymbol{A}_l \rangle = 0$ whereas $\langle \boldsymbol{A}_c \rangle \neq 0$. Therefore our conclusion is that the local and convective accelerations $\boldsymbol{A}_l$ and $\boldsymbol{A}_c$ are not approximately the same in magnitude and anti-aligned, but that the fluctuations around their mean values are. This conclusion is effectively the same as that of [13] except that in HIT the mean values of the local and convective accelerations are both zero. The correct generalisation of the result obtained by [13] for HIT is therefore the statement that it is the fluctuations of the convective and local accelerations around their means which approximately cancel each other and not the convective and local accelerations themselves.

6.3. *Quadratic mean profiles of a*

We now turn our attention to the profiles of the variances of the acceleration $\boldsymbol{a}$ and of its constituent components $\boldsymbol{a}_l \equiv \partial \boldsymbol{u'}/\partial t$ and $\boldsymbol{a}_c \equiv \boldsymbol{u'} \cdot \nabla \boldsymbol{u'}$. Of these, only the convective acceleration $\boldsymbol{a}_c$ is Galilean invariant and so we calculate all quantities in the frame where the walls of the channel are stationary.

On the basis of the conventional type of scaling arguments already used in this work, we may expect the rms of $\boldsymbol{a}_c$ to scale as follows in the intermediate log-like layer:

$$\boldsymbol{a}_c \equiv \boldsymbol{u'} \cdot \nabla \boldsymbol{u'} \sim u_{rms} \frac{u_\eta}{\eta} \tag{39}$$

$$\sim u_\tau \frac{u_\tau z_+^{-1/4}}{\delta_\nu^{3/4} z_+^{1/4}} \tag{40}$$

$$\sim \frac{u_\tau^2}{\delta_\nu} z_+^{-1/2} \tag{41}$$

where u_{rms} is a characteristic fluctuating velocity rms. Similarly we may expect the rms of $\boldsymbol{a}_l$ to scale as

$$\boldsymbol{a}_l \equiv \frac{\partial \boldsymbol{u'}}{\partial t} \sim U \frac{u_\eta}{\eta} \tag{42}$$

$$\sim u_\tau \frac{u_\tau z_+^{-1/4}}{\delta_\nu^{3/4} z_+^{1/4}} \tag{43}$$

$$\sim \frac{u_\tau^2}{\delta_\nu} z_+^{-1/2} \tag{44}$$

in the intermediate log-like layer.

These scalings are neither clearly consistent nor clearly inconsistent with the results plotted in figures 14b and 14c. In particular Figure 14 shows that the rms values of all three quantities normalised by u_τ^2/δ_ν are larger for our larger Reynolds number at all distances from the wall. This is inconsistent with (41) and (44) but may be due to our relatively low Reynolds numbers, an issue which cannot be resolved in this paper. Also, there are no clear power-law dependencies on z_+ at distances $z_+ \geq 30$. In fact, if the figures are studied carefully the profiles in all three directions appear different for all three terms and it is unclear at this stage how these differences might change with Reynolds number. The one conclusion,

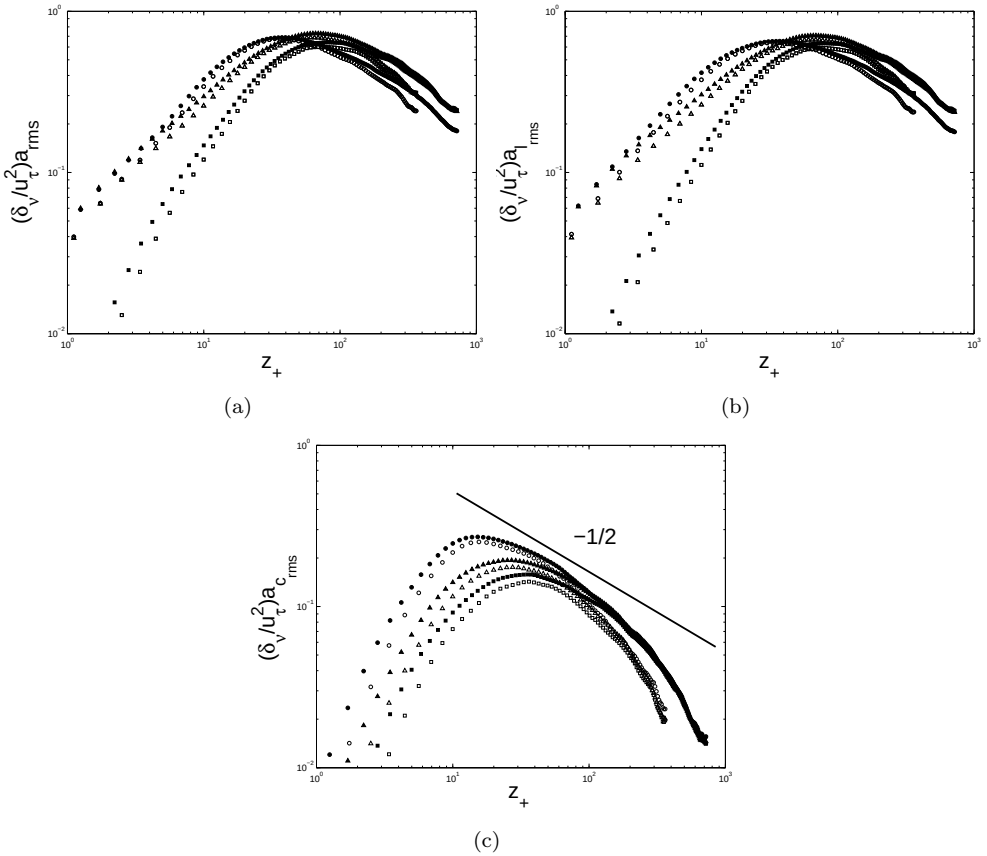

Figure 14. Rms value of terms constituting the acceleration due to the fluctuating velocity. Circles indicate streamwise, triangles spanwise and squares wall normal. Open and filled symbols are for $Re_\tau = 360$ and 720 respectively. (a) total acceleration a_{rms}, (b) local acceleration $a_{l,rms}$ and (c) convective acceleration $a_{c,rms}$.

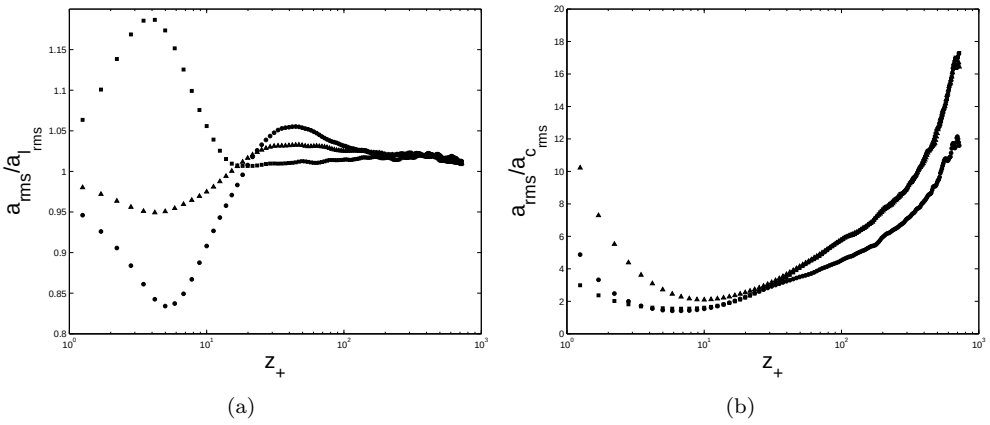

Figure 15. Ratio of rms values of acceleration due to the fluctuating velocity terms. Circles indicate streamwise, triangles spanwise and squares wall normal. (a) $a_{rms}/a_{l,rms}$, (b) $a_{rms}/a_{c,rms}$. $Re_\tau = 720$.

however, which is clear from our results, as can be seen in figure 14 but much more clearly in figure 15, is that $|\boldsymbol{a}_c| \ll |\boldsymbol{a}_l| \sim |\boldsymbol{a}|$ in the region where $z_+ \geq 20$. This conclusion is in agreement with (39) and (42) and the fact that $u_{rms} \ll U$.

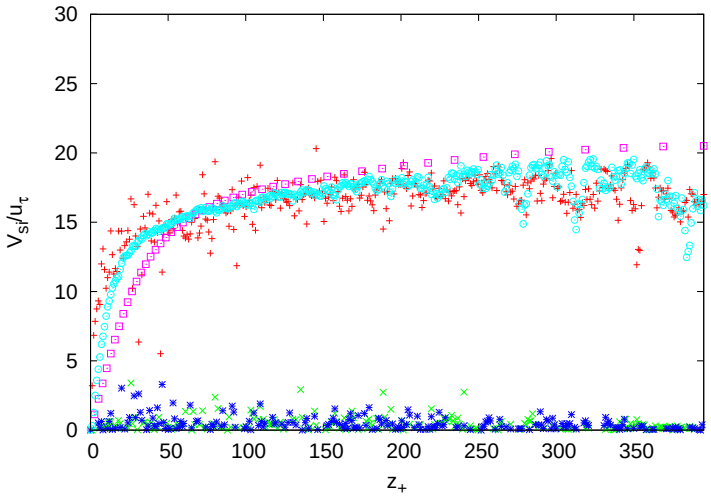

Figure 16. Mean velocities for $Re_\tau = 360$. Red (+) - $\langle \boldsymbol{V}_{sx} \rangle$. Green (x) - $\langle \boldsymbol{V}_{sz} \rangle$. Blue (∗) - $\langle \boldsymbol{V}_{sy} \rangle$. Light blue (○) - $\langle u \rangle_{sp}$. Purple (□) - $\langle u \rangle$.

7. Stagnation point velocity and acceleration statistics conditional on stagnation points

In this last section we give a few preliminary results on the statistics of stagnation point velocities $\boldsymbol{V}_s$ in a turbulent channel flow. Our purpose is only to introduce the topic and motivate future studies.

We use (6) to calculate $\langle \boldsymbol{V}_s \rangle_{sp}$ where the notation $\langle \ldots \rangle_{sp}$ means an average over stagnation points within a thin slice parallel to the channel walls. These slices are of dimension $L_x \times L_y \times \delta_z$ where δ_z is the thickness of the slice. The number of stagnation points in such slices as a function of the slice's distance z from the closest channel wall are given in figure 5. In figure 16 we plot the profiles of the three components of $\langle \boldsymbol{V}_s \rangle_{sp}$ as functions of z_+. It is clear that stagnation points do not have a clear mean motion towards the walls or in the spanwise direction. However, they do move on average along the streamwise direction with an average speed which seems to equal the average fluid velocity at these points, i.e.

$$\langle \boldsymbol{V}_s \rangle_{sp} = \langle \boldsymbol{u} \rangle_{sp}. \tag{45}$$

Hence, the average motion of stagnation points is as if they were fluid elements.

We now turn to the rms, or quadratic mean, profiles of the three components of $\boldsymbol{V}_s$. In HIT, the Reynolds number scaling of the variance of $\boldsymbol{V}_s$ is the ratio of the Reynolds number scaling of the variance of the acceleration $\boldsymbol{a}$ (which, in HIT, is the same as the variance of $\boldsymbol{A}$) and of the Reynolds number scaling of the variance of the fluid velocity gradients [7]. This follows from (6) as, in HIT, the velocity gradients $\boldsymbol{\nabla u'}$ and $\boldsymbol{V}_s$ are statistically uncorrelated and the acceleration statistics conditional on stagnation points do not show relevant differences from the acceleration statistics collected from the entire flow. In turbulent channel flows, however, $\boldsymbol{\nabla u'}$ and $\boldsymbol{V}_s$ are not uncorrelated. Equation (6) implies that $\langle \boldsymbol{a} \rangle_{sp} = -\langle \boldsymbol{V}_s \cdot \boldsymbol{\nabla u'} \rangle_{sp}$ and we have numerically checked that $\langle \boldsymbol{a} \rangle_{sp}$ does not vanish in the streamwise direction, very much like $\langle \boldsymbol{a} \rangle$. Hence, $\langle \boldsymbol{V}_s \cdot \boldsymbol{\nabla u'} \rangle_{sp}$ is not zero and is also not equal to $\langle \boldsymbol{V}_s \rangle_{sp} \cdot \langle \boldsymbol{\nabla u'} \rangle_{sp}$.

The lack of decorrelation between $\boldsymbol{\nabla u'}$ and $\boldsymbol{V}_s$ in turbulent channel flows means that a full study of these correlations will be needed to understand how the variances of the three components of $\boldsymbol{V}_s$ scale with z_+, the local Reynolds number of

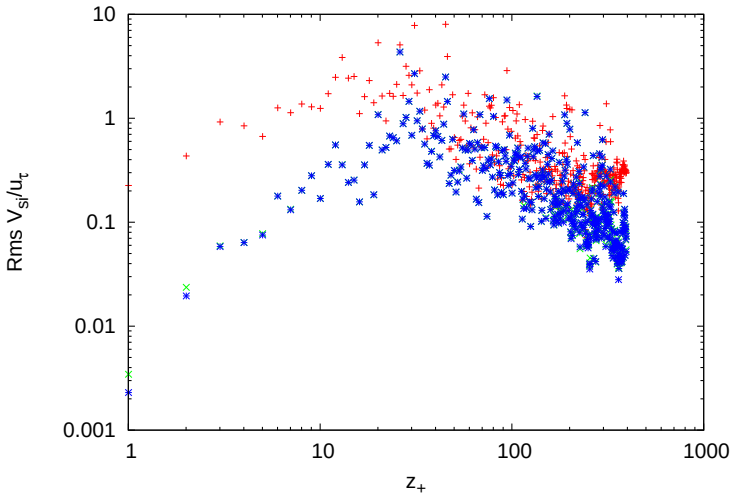

Figure 17. Rms of $\boldsymbol{V}_s$ at stagnation points for $Re_\tau = 360$.

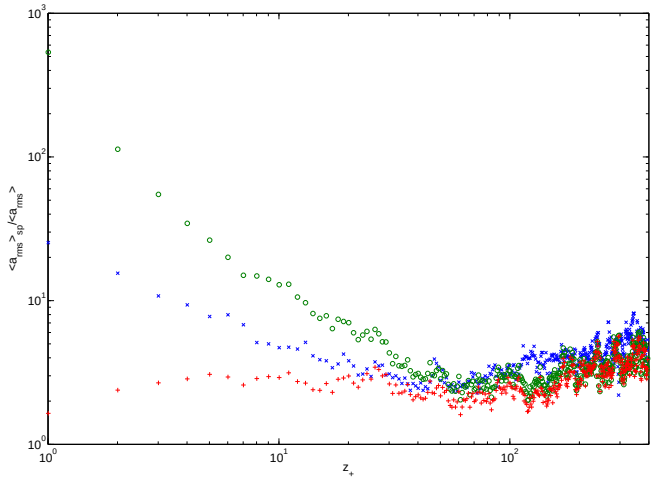

Figure 18. Ratio of a_{rms} at stagnation points and throughout the fluid for $Re_\tau = 360$. Blue (x) - streamwise direction, green (○) - wall normal, red (+) - spanwise.

the turbulence. This study is too extensive and involved to fit in this present paper, but we do nevertheless motivate it for the future by plotting in figures 17 and 18, respectively, the z_+-profiles of the rms of $\boldsymbol{V}_s$ and of the rms of $\boldsymbol{a}$ conditional on stagnation points. It is clear that the root mean squares of $\boldsymbol{V}_s$ in all three directions are commensurate with the skin friction velocity u_τ around $z_+ \approx 30$ where they peak, and it is also clear that they decrease with increasing distance from the wall in the region where $z_+ > 30$. This result is significant as it quantifies the fact that, in the local frame of reference moving with the mean stagnation point velocity, the flow topography is most unsteady in the region which might be identified with the buffer layer. The second reason which makes this result significant is its suggestion that, in the limit of very high Reynolds number Re_τ and as one moves away from the wall towards the centre of the channel, the root mean squares of $\boldsymbol{V}_s$ diminish and, presumably, eventually vanish. In this limit the local turbulence becomes approximately homogeneous isotropic and, as shown by [7], the variance of $\boldsymbol{V}_s$ does indeed tend to 0 as Reynolds number tends to infinity in HIT. Our results seem therefore to be consistent with those of [7].

Figure 18 shows that the variances of $\boldsymbol{a}$ conditional on stagnation points are higher than the unconditional variances of $\boldsymbol{a}$ and that this holds in all three directions. However, it is difficult to conclude much from this figure concerning the differences and/or similarities between the z_+-profiles of these two variances in the intermediate log-like layer, and it is also impossible to explain figure 17 from figure 18 and the statistics of $\boldsymbol{\nabla u'}$. An explanation of figure 17 will require a study which goes beyond the mean and rms profiles of this paper and considers correlations between accelerations, velocity gradients and stagnation point velocities in some detail. As this is beyond our present scope, we leave it for future study.

8. Conclusions

Our DNS provides an independent confirmation that in the range $\delta_\nu \ll z \lesssim h/2$, the number density of stagnation points is inversely proportional to the distance z from the closest channel wall. This is a property concerning toplogical statistics and it is a deeper property than the actual mean flow profile. The log-law follows from it in turbulent channel flows if the turbulent kinetic energy is independent of z in this intermediate range. Different mean flow profile shapes follow from it depending on the z-dependence that Townsend's inactive motions impart on the turbulent kinetic energy.

The stagnation points move and their motion is determined by the turbulent velocity gradients and the rate with which the turbulent velocity changes at their location. On average, stagnation points move as if they were fluid elements: the average stagnation point velocity profile coincides with the average fluid velocity profile averaged over the locations of stagnation points. The fluctuations around this average stagnation point motion peak around $z_+ \approx 30$ where they are commensurate with u_τ; they decrease with increasing distance from the wall in the region $z_+ > 30$, and they decrease with decreasing distance to the wall in the region $z_+ < 30$.

These results suggest a picture where the topology of the turbulence is just differentially swept, on average, along the channel. This differential sweeping reflects to a significant extent the mean flow profile but is nevertheless different from it. This sweeping picture relates to the sweeping decorrelation hypothesis which was originally introduced by [19] for HIT and which we reformulate here for wall-bounded turbulence following [13]'s explicit formulation in terms of the local and convective parts of the acceleration field.

In turbulent channel flow we are forced to distinguish between the acceleration $\boldsymbol{A}$ corresponding to the full fluid velocity $\boldsymbol{u}$ and the acceleration $\boldsymbol{a}$ corresponding to the fluctuating velocity $\boldsymbol{u'} \equiv \boldsymbol{u} - \langle \boldsymbol{u} \rangle$ where $\langle \boldsymbol{u} \rangle$ is the mean flow. The sweeping decorrelation hypothesis can be adapted to wall turbulence in terms of $\boldsymbol{A}$, if care is taken to recognise that the mean acceleration $\boldsymbol{A}$ is not necessarily zero. This adapted formulation states that the fluctuations of the convective and local parts of $\boldsymbol{A}$ around their means approximately cancel each other in the intermediate log-like layer. This is probably the main result of this paper and it is accompanied by our observation that in this same intermediate layer, the fluctuations of $\boldsymbol{a}$ around its mean come predominantly from the fluctuations of its local part, the convective part being negligible by comparison. As the convective part of the acceleration $\boldsymbol{a}$ is by definition zero at stagnation points, we might have expected the fluctuations of $\boldsymbol{a}$ at stagnation points to be representative of the fluctuations of $\boldsymbol{a}$ throughout. However this is not the case as the variance of $\boldsymbol{a}$ at stagnation points is significantly larger than the unconditional variance of $\boldsymbol{a}$, thus suggesting that the turbulent velocities may be more unsteady around stagnation points than they are in general.

References

[1] S. B. Pope. *Turbulent Flows*. Cambridge University Press, 2000.
[2] V. Dallas, J. C. Vassilicos, and G. F. Hewitt. Stagnation point von kármán coefficient. *Phys. Rev. E*, 80(4):046306, 2009.
[3] A. A. Townsend. Equilibrium layers and wall turbulence. *Journal of Fluid Mechanics Digital Archive*, 11(01):97–120, 1961.
[4] A. A. Townsend. *The Structure of Turbulent Shear Flow*. Cambridge University Press, 1976.
[5] S. Hoyas and . Jiménez. Scaling of the velocity fluctuations in turbulent channels up to $Re_\tau = 2003$. *Physics of Fluids*, 18(1):011702, 2006.
[6] H.E. Fiedler. Coherent structures in turbulent flows. *Progress in Aerospace Sciences*, 25(3):231 – 269, 1988.
[7] S. Goto, D. R. Osborne, J. C. Vassilicos, and J. D. Haigh. Acceleration statistics as measures of statistical persistence of streamlines in isotropic turbulence. *Phys. Rev. E*, 71(1):015301, 2005.
[8] P. Vedula and P. K. Yeung. Similarity scaling of acceleration and pressure statistics in numerical simulations of isotropic turbulence. *Physics of Fluids*, 11(5):1208–1220, 1999.
[9] S. B. Pope. Lagrangian pdf methods for turbulent flows. *Annual Review of Fluid Mechanics*, 26:23–63, 1994.
[10] B. L. Sawford. Reynolds number effects in lagrangian stochastic models of turbulent dispersion. *Physics of Fluids A: Fluid Dynamics*, 3(6):1577–1586, 1991.
[11] P. K. Yeung and S. B. Pope. Lagrangian statistics from direct numerical simulations of isotropic turbulence. *Journal of Fluid Mechanics Digital Archive*, 207:531–586, 1989.
[12] P. K. Yeung. One- and two-particle lagrangian acceleration correlations in numerically simulated homogeneous turbulence. *Physics of Fluids*, 9(10):2981–2990, 1997.
[13] A. Tsinober, P. Vedula, and P. K. Yeung. Random taylor hypothesis and the behavior of local and convective accelerations in isotropic turbulence. *Physics of Fluids*, 13(7):1974–1984, 2001.
[14] A. La Porta, G. A. Voth, A. M. Crawford, J. Alexander, and E. Bodenschatz. Fluid particle accelerations in fully developed turbulence. *Nature*, 409:1017–1019, February 2001.
[15] N. Mordant and A. M. Crawford and E. Bodenschatz Experimental lagrangian acceleration probability density function measurement. *Physica D: Nonlinear Phenomena*, 193(1-4):245 – 251, 2004.
[16] J. Mann, S. Ott, J. Berg, and B. Lüthi. The Correlation Between Velocity and Acceleration in Turbulence. In M. Oberlack, G. Khujadz, S. Günther Weller, Tanja, M. Frewer, J. Peinke, & S. Barth, editor, *Progress in Turbulence, II*, p 95, 2007.
[17] R. J. Hill. Scaling of acceleration in locally isotropic turbulence. *Journal of Fluid Mechanics*, 452:361–370, 2002.
[18] G. Gulitski, M. Kholmyansky, W. Kinzelbach, B. Luthi, A. Tsinober, and S. Yorish. Velocity and temperature derivatives in high-reynolds-number turbulent flows in the atmospheric surface layer. part 2. accelerations and related matters. *Journal of Fluid Mechanics*, 589:83–102, 2007.
[19] H. Tennekes. Eulerian and lagrangian time microscales in isotropic turbulence. *Journal of Fluid Mechanics Digital Archive*, 67(03):561–567, 1975.
[20] K. T. Christensen and R. J. Adrian. The velocity and acceleration signatures of small-scale vortices in turbulent channel flow. *Journal of Turbulence*, 3:23, April 2002.
[21] Z. Hu, C. L. Morfey, and N. D. Sandham. Sound radiation in turbulent channel flows. *Journal of Fluid Mechanics*, 475:269–302, 2003.
[22] L. Kleiser and U. Schumann. Treatment of incompressibility and boundary conditions in 3-D numerical spectral simulations of plane channel flows. In *Conference on Numerical Methods in Fluid Mechanics, 3rd, Cologne, West Germany, October 10-12, 1979, Proceedings. (A80-38252 15-34) Braunschweig, Friedr. Vieweg und Sohn Verlagsgesellschaft mbH, 1980, p. 165-173.*, pages 165–173, 1980.
[23] J. Kim, P. Moin, and R. Moser. Turbulence statistics in fully developed channel flow at low reynolds number. *Journal of Fluid Mechanics Digital Archive*, 177:133–166, 1987.
[24] R. A. Antonia and J. Kim. Low-Reynolds-number effects on near-wall turbulence. *Journal of Fluid Mechanics*, 276:61–80, 1994.
[25] H. Abe, H. Kawamura, and Y. Matsuo. Direct numerical simulation of a fully developed turbulent channel flow with respect to the reynolds number dependence. *Journal of Fluids Engineering*, 123(2):382–393, 2001.
[26] A. E. Perry and M. S. Chong. On the mechanism of wall turbulence. *Journal of Fluid Mechanics Digital Archive*, 119:173–217, 1982.
[27] J. Dávila and J. C. Vassilicos. Richardson's pair diffusion and the stagnation point structure of turbulence. *Phys. Rev. Lett.*, 91(14):144501, 2003.
[28] A. Tsinober. *An Informal Conceptual Introduction to Turbulence*. Springer, 2009.
[29] W. Heisenberg. Zur statistischen Theorie der Turbulenz. *Zeitschrift fur Physik*, 124:628–657, 1948.
[30] A. M. Yaglom. On the acceleration field in a turbulent flow. *Dokl. Akad. Nauk SSSR*, 67(5):795–798, 1949.